Physica Scripta. Vol. 28, 193–200, 1983

Beam-Foil Study of Titanium in the EUV Using Foils of Different Materials

S. Bashkin*, E. Träbert, P. H. Heckmann, H. v. Buttlar

Experimentalphysik III, Ruhr-Universität Bochum, Postfach 102148, D-4630 Bochum 1, F.R. Germany

and

K. Brand

Dynamitron-Tandem-Laboratorium, Ruhr-Universität Bochum

Received March 8, 1983; accepted April 29, 1983

Abstract

The ultraviolet spectrum (λ8–60 nm) of highly ionized titanium after foil excitation of 15 and 20 MeV fast ions has been recorded. A number of new lines, mainly in sodiumlike Ti XII, are identified. Line intensity ratios and decay curves are measured in selected cases. Using foils of different materials, relative intensities of yrast transitions $n = 3$–6 are evaluated and intercompared with the aid of cascade models. Decay curves of yrast levels are studied for resonance effects in the population mechanism. Little evidence is found for such effects.

1. Introduction

In the field of beam-foil spectroscopy, the interaction process of the ion beam with the exciter foil has found fresh interest since recent spectroscopic evidence [1, 2] indicates some sort of a resonant electron capture or excitation to excited states of high principal quantum number n. This effect has been observed as an overpopulation of these states when compared to population laws which require populations after foil excitation which decrease smoothly with n. The principal quantum number of the affected states supposedly lies close to the net charge ζ of the core of the ion leaving the foil. The effect has been explained in terms of a binding energy and velocity matching of electrons in the foil material with the tranversing ion [2–4]. However, present experimental data are limited to some few-electron ions of fairly low Z (up to $Z = 8$) [1] and rather slow heavy ions (Ar, Kr up to $q = 7+$, at 2 MeV [2], and Xe at 4 MeV [5]). A recent experiment on fast oxygen ions (40–60 MeV [6]) even shows an opposite effect, namely the underpopulation of certain excited states.

In the present experiment intermediate charge states and ion beam energies were studied. Titanium was chosen because its EUV spectrum after foil excitation had not been measured before, although it has been investigated using other light sources in connection with fusion reactor problems. Extensive spectral tables covering mostly low-lying levels and transitions between these are available [7–12].

To study the n-dependence of the initial population after foil excitation by spectroscopic means, the wavelength dependence of the relative detection efficiency of the spectrometer has to be known. Such a spectrometer, calibrated for part of the EUV range, is available at Bochum [13, 14]. The calibration range (λ13–75 nm), however, only covers transitions up to $n = 6$ for ions of, say, Na-like Ti XII. Among these levels are the $3p$ and $3d$ levels for which molecular orbital (MO) processes have been shown to be of major influence on the population after foil excitation [2, 15].

Resonant excitation would be expected for levels around $n = 12$–16 (for Ti XII). Transitions originating from these levels are in the visible and near ultraviolet spectral region and thus outside the range of the spectrometer. The decays of these states, however, will transfer information on the initial populations to lower levels, and any prominent effects for specific high-lying levels occuring when changing the foil material ought to show up in the cascade repopulation of the lower levels the decay of which can be studied with the available spectrometer.

2. Experimental set-up

2.1. *Accelerator*

The experiment was carried out at the Bochum 4 MV Dynamitron tandem accelerator laboratory. $^{48}TiH^-$ ions were produced out of a high intensity sputter ion source originally developed by Middleton [16]. The sputter cathode consisted of a cylindrical piece of pure titanium, 6 mm diameter by 6 mm long. The cathode was loaded with hydrogen and carefully mounted to the freon-cooled copper cathode holder in order to optimize heat transfer from the titanium to the copper. The source produced currents of about 2 μA of $^{48}TiH^-$; the peak current was 3.5 μA. The source output spectrum always contained negative hydrogen ions tenfold higher in intensity than the titanium hydride.

For the envisaged population studies, the simple sodium-like spectrum of Ti^{11+} (Ti XII) was considered particularly advantageous. Ti^{11+} is produced by foil traversal of fast ions; the $q = 11$ charge state fraction exceeds 10% in the beam energy range 11–36 MeV [17, 18]. A beam energy of 20 MeV would have been the optimum for the production of Ti^{11+} ions. This energy corresponds to particles with charge $q = 4+$ at the high energy end of the accelerator. The strength of the analyzing and switching magnets, however, is not sufficient to handle $^{48}Ti^{4+}$ at 20 MeV. Therefore most of the data have been recorded using 15 MeV ions, with beam currents of up to 1 μA Ti^{4+}.

Later on, an additional gas stripper was introduced between

* Senior U.S. Scientist von Humboldt Awardee, permanent address: Department of Physics, University of Arizona, Tucson, AZ 85721, U.S.A.

the high energy end of the accelerator and the analyzing magnet. This device stripped Ti^{4+} ions at 20 MeV to produce Ti^{8+} ions with 50% efficiency. The experimentally determined stripping yield is in agreement with expectation [17]. Beam currents of 450 nA of Ti^{8+} (600 nA after foil traversal) were achieved at the experimental site.

2.2. *Foils*

In the target chamber, the ions traversed thin foils of either pure carbon (10 $\mu g\,cm^{-2}$) or of other materials on a carbon backing. Carbon backed foils were chosen because their lifetime in the beam is longer than for foils without backing and because only the rear suface of the foil is thought to be of importance in the electron pick-up model. Carbon foils were produced by vacuum deposition from an arc discharge. For the composite foils, coatings of about 2 $\mu g\,cm^{-2}$ of B, Al or Au were evaporated onto one side of such carbon foils. As the thin coated foils showed a tendency to break under ion bombardment, thicker foils ($< 20\,\mu g\,cm^{-2}$) were used later on. To permit intercomparison of results from different foils, foils of each type and from the same production batch were mounted with the coating pointing up- or down-stream to cancel possible foil thickness effects on the excitation mechanism.

When trying to mount metal-coated foils from the floating liquid (water) onto the foil holders, a problem was encountered: The foils were easily caught with the carbon side onto the holder, but flipped over instantaneously when trying to mount them the other way. This was remedied by covering the foil holder surface with pencil graphite.

The foil holders were made of brass with a circular hole (4 mm diameter) for the foil. An aperture in front of the foil mount limited the beam spot to 3 mm in diameter; it usually was less because of focusing.

Under ion impact the C/Au foils had about the same lifetime as pure C foils. This may be due to the small number of atomic layers of gold (about 4) of the coating at 2 $\mu g\,cm^{-2}$. The C/Al foils broke after about half that irradiation dose, whereas the C/B foils withstood the ion beam for short periods only which rendered spectroscopy quite difficult.

In the vacuum chamber a pressure of about 5×10^{-4} Pa was maintained using turbopumps.

2.3. *Detection system*

After traversing the exciter foil. a fraction of the fast ions is excited and subsequently emits electromagnetic radiation and/or electrons on its way down-stream. In this experiment, a grazing incidence monochromator (McPherson 247) equipped with a gold-coated 600 l mm^{-1} grating ($R = 2.2$ m, $\alpha = 86°$) and a channeltron detector views the ion beam at right angles and records the EUV spectrum from 8 to 60 nm. Details of the set-up may be found elsewhere [19]. The relative detection efficiency curve of the monochromator has been established in the range λ13.5–75 nm [13, 14].

The experimental set-up also permitted the recording of decay curves. From the curves, initial amplitudes of individual decay contributions are evaluated [19, 20].

3. Observations with pure carbon foils

3.1. *Spectra and wavelengths*

Because of the foil lifetime problem with the composite foils, spectral scans with narrow slits of 80 or 50 μm (linewidths (FWHM or 0.05 and 0.035 nm, respectively) were possible only with pure carbon foils. The endurance of these foils was improved by laser treatment prior to ion beam exposure [21]. The high resolution spectra extended over λ8.8–52.6 nm (Fig. 1). This range was chosen in order to cover most of the 3–4 transitions in Ti^{11+} and neighbouring charge states and the $n = 5\text{–}n' = 6$ yrast transition in Ti XII. As expected from the charge state distribution at 20 MeV [17], the lines of sodium-like titanium (Ti XII) dominate the spectrum. Other identified lines belong to the spectra Ti XIV (F I-like), Ti XIII (Ne I-like), Ti XI (mg I-like), and Ti X (Al I-like). Some lines of lower charge state spectra coincide with weak spectral structures but are too weak for an unequivocal assignment.

The spectrometer was calibrated using well-known and resolved lines of Ti XII, XI and X [6–8, 11, 12, 22] as standards. The calibration curve reproduced the wavelengths of all known lines to about 0.005 nm. This is in agreement with an estimate of the calibration error from the statistical uncertainty of the individual line positions: Because of the nonlinear relation of wavelength and spectrometer readout, an average uncertainty of 0.3 channels in the spectrum shown in Fig. 1 corresponds to a wavelength uncertainty of 0.004 nm at the short and of 0.008 nm at the long wavelength end of that spectrum.

A number of lines which exceed the background by more than 5 standard deviations but not reported from other light sources or not classified [6–11] are listed in Table I. As the population mechanism of the beam-foil interaction is rather non-selective and is known to populate highly and multiply excited states to a much greater extent than other light sources, most of the new lines will represent transitions between levels in Ti X–XIII, with principal quantum numbers 4 to 7. In case of Ti XII we applied Edlén's formulae [22] to correct hydrogenic term values [23] for the polarization of the electron core; the results are several identifications of Rydberg lines in this spectrum. Because of a lack of a similarly simple and valid formalism for systems with more electrons (say Mg I-like), the other classifications in Table I are based on term values and extrapolation of term series given in [11] but are considered to be tentative.

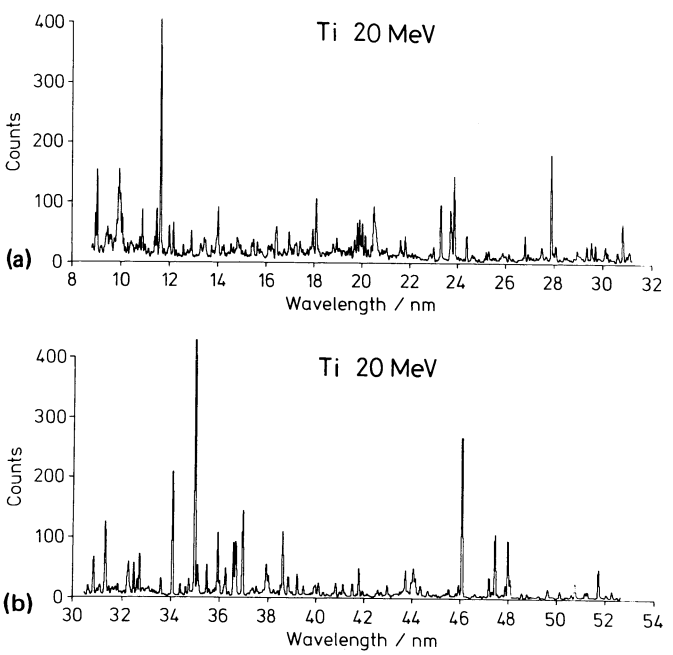

Fig. 1. Spectrum of titanium at beam energy 20 MeV after excitation by carbon foil (a) λ = 8.5–30 nm, (b) λ = 30–52 nm. Spectrometer slit width 50 μm, instrumental line width (FWHM) 0.03 nm.

Table I. *List of significant unidentified and newly classified spectral lines of Ti X–XIII in the range 8.8–52 nm*

Wavelength λ/nm	Comment		Identification	
	Precision	Intensity	Spectrum	Transition
12.022	B	mw	XIII	$4s\ ^3P^0–6p\ ^3P$
13.316	B	mw		
13.465	B	mw	XI	$3s4p–3s7d$
			XI	$3p3d\ ^1F^0_3–3p4f\ ^1G_4$
13.515	B	mw	XI	$3s3d–3s4f$
13.770	B	mw		
14.206	B	mw	XIII	$4p\ ^3P–6s\ ^3P^0$
14.567	B	mw		
14.82	C	mw	XIII	$4d\ ^3D^0–6f\ ^3F$
15.17	C	w		
15.426	C	mw		
15.498	B	mw	XIII	4–6
15.66	B	mw	XI	$3s4p\ ^3P^0–3s6d\ ^3D$
16.116	B	mw		
16.184	B	mw	XI	$3s4p–3s6d$
16.245	B	mw	X	$3s^24s–3s^26p$
16.77	C	w		
17.217	B	w		
17.286	B	w	XIII	$4s\ ^3P^0–5p\ ^3P$
17.434	B	mw	XIII	$4p\ ^1P–5d\ ^1P^0$
17.738	C	w		
17.848	C	w		
18.814	B	mw	XIII	$4s\ ^1P^0–5p\ ^1P$
18.971	B	mw	XIII	$4p\ ^3P–5d\ ^3D^0$
19.07	C	w	X	$3s^24p–3s^25d$
19.12	C	w		
19.39	C	w	XI	$3s4f–3s6f$
19.471	B	w	XI	$3p4s–3p6p$
19.562	B	mw		
19.707	A	mw		
19.829	A	m	XIV	4–5?
19.916	A	m		
20.037	A	m	XI	$3p4d\ ^3D–3p6f$
20.408	B	mw		
20.510	A	m		
20.58	C	m		
21.042	C	w	XI	$4f–6g$
21.689	C	w	XI	$3s4p\ ^3P^0–3s5d\ ^3D$
23.005	B	mw	X	$3s^24s\ ^2S–3s^25p\ ^2P^0$
23.718	A	m		
23.776	A	m	XIII	$4d–5f$
23.868	A	s		
25.295	B	mw	XII	$4d–5f$
25.57	C	w	X	$4f–6g$
25.75	C	w		
26.14	C	w		
26.814	B	m		
26.935	B	w	X	$4p–5d$
27.512	B	mw	XI	$3p4s–3p5p$
27.904	A	s	XII	$4f–5g$
28.43	C	w	XI	$3s4p–3s5s$
29.369	B	m		
29.554	B	m		
29.713	B	m		
30.117	B	m		
30.209	B	w	XI	$3s5p–3s7d$
30.98	C	w	XIII	$5p\ ^1P–6d\ ^1P^0$
31.09	C	w		
31.319	A	s	XI + unknown	
31.34	C	w	XIII	$5p\ ^1D–6d\ ^1P^0$
31.47	C	w		
31.61	C	w		
31.73	C	w	X	$4d–5f$
31.820	B	w		
32.254	B	m	XI	$3s4f–3s5g$
32.481	A	m		
32.615	B	mw		

Table I. (*Continued*)

Wavelength λ/nm	Comment		Identification	
	Precision	Intensity	Spectrum	Transition
33.591	B	m		
34.385	B	mw		
34.613	B	mw	XIII	$5p\ ^3D–6d\ ^3F^0$
34.749	B	mw		
35.11	B	w		
35.481	A	m	XI	$3s5d–3s7f$
35.58	C	w	X	$4p–5s$
35.930	A	s		
36.02	B	w		
36.258	B	m		
36.575	A	s		
36.667	A	s		
36.956	A	s	XIII	$5s\ ^1P^0–6p\ ^1P$
37.36	C	w		
37.52	C	w	XI	$3p4p\ ^3P–3p5d\ ^3D^0$
37.930	B	m		
38.013	B	mw		
38.847	B	mw		
39.220	B	mw	X	$4f–5g$
39.477	B	w		
39.97	C	w		
40.105	B	w		
41.130	B	w		
42.58	C	w		
42.71	C	w	XI	$3p4p\ ^3P–3p5s\ ^3P^0$
43.720	B	m	XI	$3s5p–3s6d$
			XIII	$3s\ ^3P^0_2–3p\ ^3P_2$
			XIII	$5p\ ^3P–6s\ ^3P^0$
44.045	B	m	XIII	5–6
44.14	C	mw		
44.344	C	w		
45.525	C	w	XI	$3s4s\ ^3S–3p4s\ ^3P^0$
45.934	B	mw		
46.85	C	w	XII	$5d–6f$
47.207	A	m		
47.872	A	mw		
48.077	A	m		
48.565	B	w		
49.627	B	w		
50.128	C	w		
50.62	C	w		
50.761	B	mw		
51.17	C	w		
51.26	C	w	XII	$5f–6g$
51.722	A	m	XII	$5g–6h$
52.04	C	w	XII	$5g–6f$

Experimental uncertainty of wavelength determination. A: ± 0.005 nm, B: ± 0.01 nm, C: ± 0.02 nm. Intensity: w, weak; mw, weak to medium; m, medium; s strong.

Several groups of medium or even strong lines stand out (near 20 nm, near 36 nm, near 48 nm) which could not be identified on the basis of available data on Ti.

One obvious misidentification has been found: A line at λ26.015 nm has been listed by Kelly and Palumbo [8] as belonging to the transition Ti XII $4p–5s$. A line of this wavelength does not appear in our spectra. It does not fit into the term scheme given by Bashkin and Stoner [11] either which is otherwise consistent within the *ns* and *np* term series as judged from the quantum defect of the levels. The term scheme would suggest wavelengths of λ25.528 and 25.745 nm for the $4p–5s$ transitions. We find rather weak lines at 25.48, 25.57 and, a little stronger, at 25.75 nm. If the λ25.75 nm line was to be identified with the $4p_{3/2}–5s$ transition, then the intensity

ratio would be wrong. Hence we do not consider the term values of [11] to be accurate enough for predictions of proper wavelength values for transitions among levels with $n \geqq 4$.

3.2. *Intensities and decay curves; population of low-lying states*

The spectra at 15 and 20 MeV beam energy are rather similar and reflect the shift of the charge state distribution with energy. The absence of dramatic changes indicates that no specific excitation channel is opened or closed within this range. Such an effect was reported for neon-like and sodium-like Cl [15] and explained in terms of the MO mechanism.

When obtaining intensity information from the beam-foil light source, it is important to keep in mind that with time-resolved spectroscopy the observed intensity of a line depends on the width and position of the spatial detection window of the monochromator (which transforms to a time window with respect to the decay-in-flight of the ions [19, 20, 24] and on the replenishment from higher-lying levels.

Several authors (a.o. [25–28]) have applied computer simulations based on cascade schemes of the Na I isoelectronic sequence with theoretical transition probabilities (see, e.g., [29, 30]). The probabilities for transitions from high-lying levels can usually be obtained from Coulomb approximation calculations (e.g., [29]) with sufficient accuracy. Whereas for inter-shell transitions the Coulomb approximation is expected to give a good estimate of the transition rates, the case is different for transitions between $n = 3$ states ($3s$–$3p$–$3d$). The lifetime of the $3p$ level in Ti XII, for example, has been calculated to be 229 ps [30] or 207 ps [29]. Both calculations neglect the considerable finestructure splitting of the $3p$ state, which amounts to about 4% of the transition energy. The difference in the lifetimes of the finestructure levels will be even larger: An interpolation of the calculations by Flower and Nussbaumer [31] for Ca and Fe yields lifetimes of 198 ps ($3p_{3/2}$) and 225 ps ($3p_{1/2}$) for the Ti XII $3p$ finestructure levels, the weighted average of 207 ps being in agreement with Lindgård and Nielsen [29]. An interpolation formula by Edlén [22] for line strengths calculated by Weiss [32] yields 199 and 227 ps. This agrees with the result of Hartree–XR calculations which yield 198 and 221 ps [33].

For the $3d$ states, a multiplet lifetime of 88.8 ps [29] and individual lifetimes of 76 ps for the $3d_{3/2}$ state and 82 ps for the $3d_{5/2}$ state [31] are predicted, which is in agreement with other authors [22, 32, 33]. The $3d$ lifetime has not been measured in this experiment, but in an experiment on Fe [28] the data of Flower and Nussbaumer agreed with experimental results.

In an earlier study of simulations of the $3p$ decay [25] it was found that in spite of the very strong cascades, the $3p$ mean life can be detected in the decay curve. Present simulations of the $3p$ decay involve a cascade model of all levels up to $n = 6$, the $n = 7$ levels with $l > 2$, and the yrast levels ($l = n - 1$) up to $n = 15$. The transition rates for Ti XII levels up to $n = 7$ are taken from [29] (with the data for $n = 3$ obtained from [31–33]), and the lifetimes of the yrast levels up to $n = 12$ are scaled from the hydrogenic values of [29] by ζ^4. Lifetimes of higher-lying levels are approximated from Omidvar [34]. Initial populations according to population laws $(n - n_0)^{-\alpha} \cdot f(l)$ with $n_0 = 0$ or 1, exponents $\alpha = 2$, 3 or 4, and $f(l) = (2l + 1)$ or l^2 have been applied to the cascade model. A common result is a dominant slope of the simulated $3p$ decay curve corresponding to 215 ± 20 ps, independent of the particular population law, with a primary $3p\ ^2P^0_{3/2}$ lifetime of 200 ps in the model. An evaluation of the decreasing part of the experimental decay curve of the $3p\ ^2P^0_{3/2}$ state ($\lambda = 46.075$ nm [22]) indeed yields a main component of decay constant 225 ± 10 ps, plus a slow cascade (see Fig. 2).

Whereas the steepest-slope theorem only yields an upper limit of the lifetime of interest, an evaluation of the complete decay curve, that is inclusive of the section that is distorted owing to the spatial/temporal detection window as well as to fast growing-in cascades, provides more valuable information. A three-exponential plus detection window analysis of the decay curve shown in Fig. 2 yields components with time constants (200 ± 10) ps, (100 ± 10) ps, and (400 ± 60) ps, with initial amplitude ratios 124 : − 85 : 14.

If the second component is associated with the lifetime and initial population of a single feeding state ($3d$), the initial populations of $3d$ and $3p$ states would rate as $N^0_{3d}/N^0_{3p} = 1.2/1$, a result derived using Curtis' cascade mnemonics [35] for a few-level system. From this, the ratio of sum intensities of the line multiplets $3s$–$3p$ and $3p$–$3d$ can be predicted which, however, differs from the measured intensity ratio (Fig. 1) by a factor of 3. This shows that the above three-component treatment of the Ti XII $3p$ decay curve is not realistic. The fast cascades along the yrast line with their very short lifetimes ($4f$: 3.2 ps, $5g$: 11.3 ps, $6h$: 29.3 ps, etc.) and cascades from states with $l < n - 1$ are not explicitly represented in that decay analysis. Therefore the 100 ps cascade represents a multitude of cascades faster than the primary decay: that means it comprises cascades from levels up to about $n = 8$ ($\tau(8k) \simeq 130$ ps); the slow cascade component represents contributions from yrast decays with $n > 8$.

A correct description of the decay curve requires knowledge of the cascade pattern and of the initial population of the contributing levels. The former can be calculated [29, 36]; the latter is not known but will be approximated in the following analysis on the basis of some measurements and educated guesses. For example, the analysis has to take into account the intensities of the $3d$–$4f$ ($\lambda = 11.65$ nm), $4f$–$5g$ ($\lambda = 27.904$ nm) and $5g$–$6h$ ($\lambda = 51.726$ nm) transitions in the yrast cascade chain through which most of the repopulation occurs.

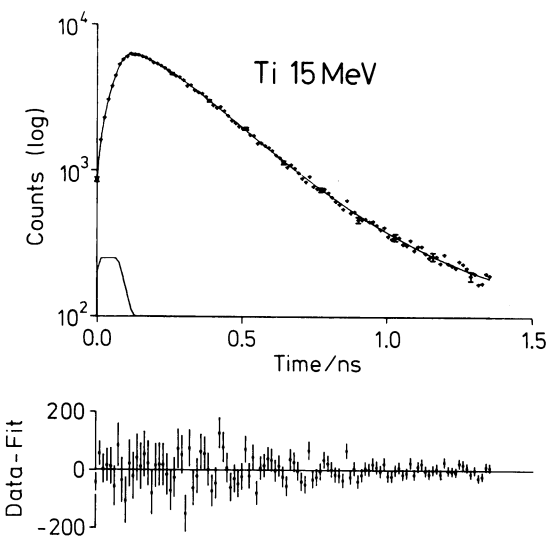

Fig. 2. Decay curve of Ti XII $3p_{3/2}$ at $\lambda = 46.075$ nm. Spectrometer slit width 0.25 mm. The geometrically determined detection window is indicated. Solid line: fit to the data using three exponential components and the window. Residual deviations of data from the fit at bottom.

Table II. *Relative intensites of decays from low-lying levels of Ti XII after excitation by a carbon foil. Data refers to spectrum of Fig. 1*

Transition	Wavelength λ/nm	Relative intensity (arbitrary units)	Normalized to $\Sigma I(3p)$
$3d$–$4f$	11.65/11.66	25 ± 5	44
$4f$–$5g$	27.904	12 ± 1.5	21
$3p_{1/2}$–$3d_{3/2}$	34.0676 [22]	18 ± 1.5	
$3p_{3/2}$–$3d_{5/2}$	34.9926 [22]	36 ± 2	99
(on account of a blend with Ti XI reduced by 10%)			
$3p_{3/2}$–$3d_{3/2}$	35.1026 [22]	4 ± 0.5	
$3s_{1/2}$–$3p_{3/2}$	46.0749 [22]	43 ± 2	100
$3s_{1/2}$–$3p_{1/2}$	47.9886 [22]	16 ± 1.5	
$5g$–$6h$	51.726	9 ± 1	15

As a first step, the observed line intensities of the 3 yrast transitions and of the 5 components of the $3s$–$3p$ and $3p$–$3d$ multiplets have to be corrected for the relative detection efficiency of the spectrometer [13]. The resulting relative intensities are listed in Table II.

As a next step, decay curves of the levels of interest are simulated and then convoluted with a trapezoidal detection window function [19]. The 0.89 mm width (at half maximum) of the detection regime corresponds to 115 ps for 15 MeV Ti ions and to 100 ps for Ti ions at 20 MeV. A point at 4/5 of the window width which represents the experimental position of the exciter foil in the plateau of the decay curve [19, 20] is chosen as a reference for comparison of line intensities.

For the Ti XII $4f$ decay near $\lambda = 11.6$ nm the approximation of the window shape by a trapezoid is poor, and the wavelength of the decay is outside the calibrated range. Therefore the error of its relative intensity is larger than in the cases $5g$ and $6h$.

In order to obtain agreement of the simulations with the experimental results, a monotonic decrease of initial populations according to $(n-n_0)^{-\alpha}\cdot f(l)$ is assumed as suggested from general trends in beam-foil spectroscopy. It turns out that for the relative intensities of the decays from the $4f$, $5g$, $6h$ transitions the various model assumptions do not differ very much, because a time window of the order of 100 ps averages out the fast primary ($4f$, $5g$, $6h$) decays. The tails of the curves are dominated by the slower cascades which are similar in the three decays and which are well described by an effective population of high-lying yrast states as $n^{-0.75}$ which transforms to the above population law with $n_0 = 0$, $\alpha = 1.75$, $f(l) = 2l + 1$ (statistical weight). In a log–log plot $I(t)$ yields a fairly straight line which can be described by a power law $I(t) \sim t^{-\beta}$, with $\beta = (0.9 \pm 0.1)$. Similar power laws are often found for yrast decay chains in beam foil spectroscopy, but usually β has values $\gtrsim 1.5$ [37]. For low-lying levels we multiply the model population of individual levels by factors which are adjusted to improve the agreement of simulated and experimental data.

Several different assumptions on the population of low-lying levels lead to similarly good fits of the $3p$ decay curve (no decay curve has been recorded for the $3d$ decay): Because of the long lifetime of the primary decay and because of the poor time resolution (detection window wing width [19, 20] 50 ps) we cannot distinguish between high population of the $3p$ and $3d$ levels and low population of the low-lying cascade levels on one hand and a less high population of the $n = 3$ levels, but rapid and strong repopulation from cascade levels. The two extreme possibilities are indicated by the limits of the shaded area in Fig. 3. The $4f$ and $5g$ decay curves suggest the population of the yrast levels to be close to the higher limit. This points to a low population of non-yrast levels with $n > 3$, a result which is in agreement with other experiments [2].

Comparison of the decay simulation with the measured decay curves reveals the following features:

– For $n \gtrsim 8$, the population of levels other than yrast levels is low. The effective population of the yrast levels follows an $n^{-(0.75 \pm 0.2)}$ dependence. This slow decrease of population with n cannot extend to arbitrarily high values of n because the sum of the initial populations must be finite.

– For yrast levels $n \lesssim 7$, the n dependence is weaker than n^{-1}.

– The $3p$ level is overpopulated by a factor of about 8 compared with the $n^{-1.75}(2l+1)$ trend of the high-n levels, whereas the $4f$, $5g$ and $6h$ levels may fall a little short of the model assumption.

– We have no explicit population information on ns levels, np levels with $n > 3$, and levels between these term series and the yrast line; our decay curves are best mimicked assuming that these levels are less populated than expected from a $n^{-1.75}(2l+1)$ model. The low intensity of spectral lines from these levels backs this assumption.

The relative populations of levels for which direct observation was possible in our study are marked in Fig. 3. A high population of p-states is often found after foil excitation (see, e.g., [37]). In case of the Ti XII $3p$ state this may indicate a vacancy promotion by the MO process, as has been suggested earlier [2, 5, 15].

The relative intensities of the Ti XII $3s$–$3p$ and $3p$–$3d$ fine-structure components can be compared with branching ratios given by theory. Without temporal resolution and concern for cascades the theoretical branching ratios [31–33] lead to

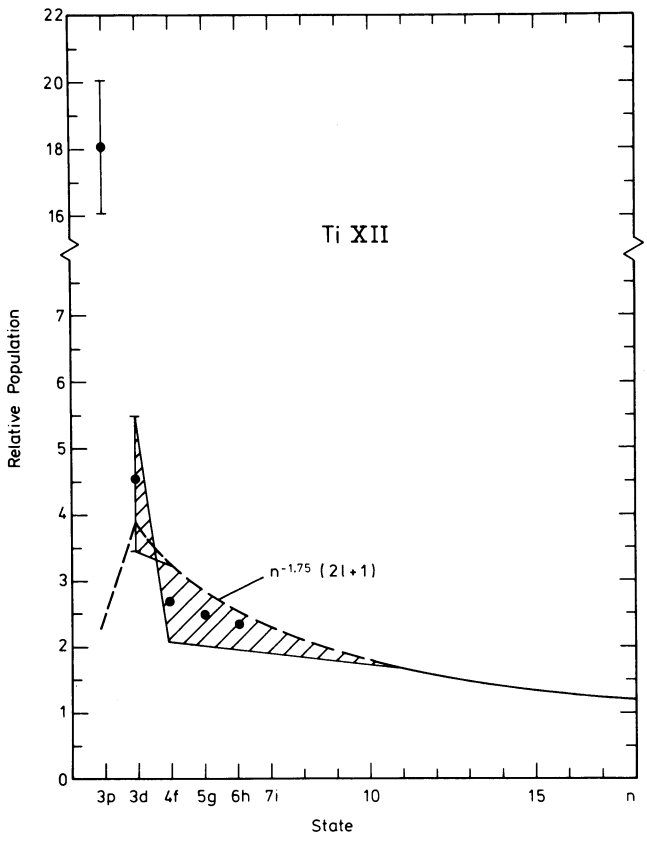

Fig. 3. Relative populations of low-lying and yrast levels and comparison with a $n^{-1.75}(2l+1)$ population law. •, levels from which direct decays have been observed.

relative intensities (components in the order of increasing wavelength) as 56:100:10 ($3p$–$3d$; j = 1/2–3/2, 3/2–5/2, 3/2–3/2) and 100:50 ($3s$–$3p$; j = 1/2–3/2, 1/2–1/2).

Simulations as above, taking account of the different lifetimes of the finestructure levels, cascades and observation window, result in predicted relative intensities as 53:100:10 ($3p$–$3d$) and 100:41 ($3s$–$3p$). The experiment shows relative intensities as (51:100:11) ($3p$–$3d$) and 100:38 ($3s$–$3p$) (see Table II). For the $3s$–$3p$ multiplet the agreement is good. The 10% difference in the lifetimes of the $3p$ finestructure levels results in a later and lower peak intensity of the $3p_{1/2}$ decay curve compared to the $3p_{3/2}$ decay and in the observed deviation from the intensity ratio 2:1. For the $3d$ decays the agreement is very good, but the $3p_{3/2}$–$3d_{5/2}$ transition coincides with a line of Ti XI (which has been allowed for in the intensity estimate), and the $3p_{3/2}$–$3d_{3/2}$ component is only partially resolved from an unknown line at $\lambda = 35.11$ nm.

3.3. *Population of high-lying states*

The decay curves of the $3d$–$4f$ and $4f$–$5g$ transitions in Ti XII have been recorded for times up to about 6 ns after excitation. This is 2×10^3 times the mean life of the $4f$ or 600 times the mean life of the $5g$ state and corresponds to the mean life of yrast states of $n \simeq 17$. An example is shown in Fig. 4.

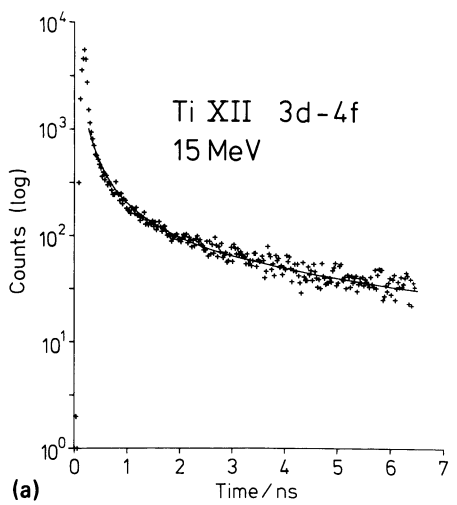

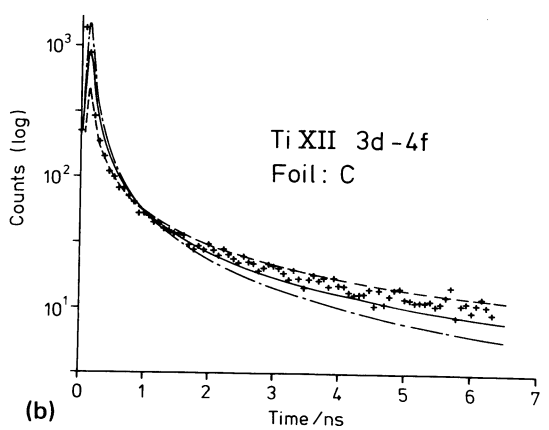

Fig. 4. Decay curve of Ti XII $4f$ at $\lambda = 11.65$ nm. (a) Experimental curve, obtained with 0.3 mm spectrometer slits. The solid line refers to a simulation with $n^{-1.75}(2l + 1)$ as explained in the text. (b) Same data but summed over every 3 channels. The solid lines refer to simulations assuming a population of the yrast levels (only) according to n^{-2} (–·–), n^{-1} (——), const. (– – –).

Assuming that the population of yrast levels is the dominant one (see some of the evidence in [2]), we have simulated decay curves on the basis of only yrast levels being populated. Figure 4 shows a good fit assuming an effective population of yrast levels according to an $n^{-0.75}$ law, valid for levels up to at least $n \simeq 16$.

If the population of a level of high n is favoured by some resonance effect [1–4] in the ion foil interaction by a factor of two, say, this shows up in the decay curve: We have tested simulating the $4f$ and $5g$ decay curves with a cascade scheme extended to yrast levels as high as $n = 20$, with the lifetimes extrapolated with the help of Omidvar's formula [34]. A hump appears in these curves at positions about twice the mean life of the overpopulated level (that is about the sum of the mean lives up to this level). An underpopulation of a group of levels can be detected equally well, it would yield a hump, too, after a curve section of steeper slope (Fig. 5). A comparison with the results of Fig. 4 shows that no such humps exist in the measured curves up to times as high as 11 ns after excitation.

4. Observations with composite foils

With composite foils, one set of experiments comprised fast spectral scans with low spectral resolution (line width (FWHM) 0.25 nm) over a wide spectral range (8–60 nm). Composite foils (C, C/B, C/Al, C/Au) were used in both orientations (see above section on foils). The aim was to survey whether the foil material had any influence on the relative populations of *low-lying* states.

The experimental result is negative: Although the relative intensity of the short-lived Ti XII $4f$ decay varies by up to a factor of two compared to the other lines in the same spectrum – this effect may simply be due to geometrical changes like bulging of the foil – the *relative* intensities of all other Ti lines from low lying levels remain virtually unchanged (± 10%).

The *light yield* (normalized to collected charge in the Faraday cup), however, differed from foil to foil. Pure carbon foils had similar light yields within 10%, but composite foils of equal elementary composition differed by as much as a factor of four. On the average the effect was small: B and Au coated foils showed a slightly lower light yield than pure carbon, Al coated foils a slightly higher one. For B and Al this holds for both orientations of the foils. For foils of similar composition, we assume the scatter in the light yield to be due to imperfect control of the foil production procedure.

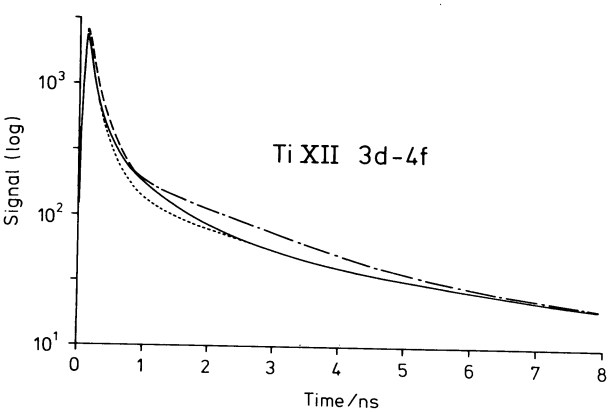

Fig. 5. Simulations of the decay curve of Ti XII $4f$ at $\lambda = 11.65$ nm showing the effect of overpopulation of specific levels. The population law assumed is $n^{-2}(2l + 1)$. ——, no overpopulation. — —, twofold overpopulation of level $n = 8$. — · —, twofold overpopulation of level $n = 12$. - - - - -, underpopulation of level $n = 10$ (factor 0.5).

A second set of experiments concerned the effect of the foil material on the population of *high-lying* levels. Similarly to the aforementioned study of pure carbon foils, the decays of Ti XII $4f$ and $5g$ levels were recorded for typically about 6 ns after excitation by composite foils (however, the short-lived B coated foils only allowed a recording time of 1 ns). The results may be summarized as follows:

– Decay curves of $4f$ and $5g$ levels are very similar, no humps are observed and thus no resonance effects in the population of yrast or near-yrast levels up to $n \sim 16$ are present.

– Curves recorded with pure C foils and C/Au foils are indistinguishable in appearance; curves from Al/C foils are rather similar, but there are less data.

– Au/C foils result in curves with the same yield as C and C/Au after about 300 ps after excitation, but significantly lower yield for shorter times. This indicates a population of levels $n \lesssim 8$ which is less by more than a factor of two compared to excitation by C foils. About the same behaviour is found using B/C foils.

– With C/Al foils the yield attributed to low-lying levels is about the same as observed with C foils, but the high-lying yrast levels are populated less.

– The population law (effectively $n^{-0.8}$) of high living levels is similar for all foils studied up to about $t = 6$ ns after excitation. This corresponds to levels as high as $n = 15$. Also C/Au and Au/C foil data which extend to $t = 10$ ns show the same decrease for the full range. The dependence of the intensity on time after excitation is equally well described by a power law $t^{-(0.8 \pm 0.1)}$ up to $t \simeq 3$ ns and $t^{-(1 \pm 0.1)}$ for $t > 4$ ns.

The present experimental evidence leads to the following conclusions:

Low-lying and high-lying levels are affected in different ways. The population law for high-lying yrast levels $8 \lesssim n \lesssim 16$ is hardly dependent on the foil material (for B, C, Al, Au). This supports the view that last-layer interactions are responsible for the population of these levels, and that the last layer may be independent of the particular foil material because it consists of contaminating materials of similar composition for all cases studied [38].

The yield of light originating from low-lying levels may vary with the foil material. Ions excited to low-lying levels in the first layers of the foil have a better chance to survive the passage through the remainder of the foil unharmed than highly-excited ions, because of their smaller geometrical size. Initial excitation to high-lying levels leads to rapid quenching when the ion is still inside the foil.

From the present data we cannot definitely exclude the validity of Veje's concept [3, 4] of resonance-enhanced population of high-lying levels. Our only evidence in favour of this concept is the slight change in the exponent of the power law approximating the long term behaviour of the yrast cascade. This change takes place around $t = 4$ ns which corresponds to yrast levels as high as $n = 14$.

These yrast levels would be bound by $E_B \simeq 10$ eV, an energy which is close to the binding energy of the $2p$ electrons in carbon [1]. Andresen et al. [1] claim that this would consequently be the energy of the valence electrons in the carboneous solid. Experimental data in the literature, however, show a wide scatter of valence electron energies in carboneous solids in the range 5–6 eV.

The position of the region of change in the power-law description of the decay curve would be expected to vary with the foil material. At our present level of significane of the data we find no such change when substituting Au for C as the rear foil surface. Previous experimental evidence in favour of this model [1, 2, 5], however, concerned level series of given angular momentum. These levels have been found to be weakly populated except for some resonance-like enhancement for a range of n values. Some experimental evidence [2] shows a rapid increase of the relative population of levels of given n towards the maximum value of l, that is the yrast level. According to our data which concern yrast levels only, the population of these levels is not dominated by a resonance effect. It might be that the Veje model is not applicable to the system and energy range studied here.

However, the data [1, 2, 5] hitherto related to resonant capture of target electrons do not extend significantly beyond the n value of maximum population. Hence what has been interpreted as a population peak may have an alternative – or additional – interpretation as an n threshold for the mechanism which is responsible for the population of high n levels. Betz [39] has proposed a model suited to explain the population of high-lying levels (weakly bound states) and convoy electrons (which are observed outside the foil at the velocity of the projectile ions) alike. The model is based on the process of electron loss to the continuum (ELC) in the foil and a subsequent recapture of the lost electrons which still move with about the velocity of the projectile. This process would be fairly independent of the foil material. At high velocities this process appears to dominate. It seems to yield a better explanation for the population of yrast levels even at low velocities, where the data on Xe [5] show a population peak for levels off the yrast line only, but a smooth variation of the population with n near the yrast line.

Acknowledgements

We are grateful to the accelerator crew for the preparatory test series and provision of the titanium beam, to Ms Scherrer for the preparation of the various foils, and to H. Hellmann, R. Hucke, B. Müller and G. Schneider for their assistance during the accelerator runs. One of us (S. B.) wishes to express his gratitude to the Alexander-von-Humboldt-Stiftung for their award and continuous support.

References

1. Andresen, B., Denne, B., Ekberg, J. O., Engström, L., Huldt, S., Martinson, I. and Veje, E., Phys. Rev. **A23**, 479 (1981).
2. Bashkin, S., Oona, H. and Veje, E., Phys. Rev. **A25**, 417 (1982); Nucl. Instr. Meth. **194**, 369 (1982).
3. Veje, E., Surf. Sci. **109**, L545 (1981).
4. Veje, E., Surf. Sci. **110**, 533 (1981).
5. Hallin, R., Leavitt, J. A., Lindgård, A., Rathmann, P. W., Vach, H. and Veje, E., Nucl. Instr. Meth. **202**, 41 (1982).
6. Betz, H. -D., Rothermel, J., Röschenthaler, D., Bell, F., Schuch, R. and Nolte, G., Phys. Lett. **91A**, 12 (1982).
7. Svensson, L. Å. and Ekberg, J. O., Arkiv Fysik **40**, 145 (1969).
8. Kelly, R. L. and Palumbo, L. J., Atomic and Ionic Emission Lines Below 2000 Ångstrøms, Hydrogen through Krypton, NRL, Washington (1973).
9. Corliss, C. and Sugar, J., J. Phys. Chem. Ref. Data **8**, 1 (1979).
10. Fawcett, B. C., Report ARU-R4, Culham (1971).
11. Bashkin, S. and Stoner, Jr., J. O., Atomic Energy Levels and Grotrian Diagrams, Vol. 2. North Holland, Amsterdam (1978).
12. Mori, K., JAERI Report 82-078 (1982).
13. Träbert, E., Heckmann, P. H., Raith, B. and Sander, U., Physica Scripta **22**, 363 (1980).

14. Träbert, E., Schneider, G. and Heckmann, P. H., Physica Scripta **27**, 407 (1983).
15. Jupén, C., Denne, B., Ekberg, J. O., Engström, L., Litzén, U., Martinson, I., Tai-Meng, W., Trigueiros, A. and Veje, E., Phys. Rev. **A26**, 2468 (1982).
16. General Ionex model 850.
17. Sayer, R. O., Rev. de Physique Appl. **12**, 1543 (1977).
18. Delaunay, B., Nucl. Instr. Meth. **146**, 101 (1977).
19. Träbert, E., Heckmann, P. H., Schlagheck, W. and Buttlar, H. v., Physica Scripta **21**, 27 (1980).
20. Träbert, E. Winter, H., Heckmann, P. H. and Buttlar, H. v., Nucl. Instr. Meth. **135**, 353 (1976).
21. Große-Kreul, B., Bukow, H. H. and Sander, U., Nucl. Instr. Meth. **193**, 645 (1982).
22. Eldén, B., Physica Scripta **17**, 565 (1978).
23. Erickson, G. W., J. Phys. Chem. Ref. Data **6**, 831 (1977).
24. Baudinet-Robinet, Y., Garnir, H. P., Dumont, P. D. and Livingston, A. E., Physica Scripta **14**, 224 (1976).
25. Crossley, R. J. S., Curtis, L. J. and Froese Fischer, C., Phys. Lett. **57A**, 220 (1976).
26. Younger, S. M. and Wiese, W. L., Phys. Rev. **A17**, 1944 (1978); Phys. Rev. **A18**, 2366 (1978).
27. Buchet, J. P., Buchet-Poulizac, M. C., Denis, A., Desesquelles, J. and Druetta, M., Phys. Rev. **A22**, 2061 (1980).
28. Träbert, E., Jones, K. W., Johnson, B. M., Gregory, D. C. and Kruse, T. H., Phys. Lett. **87A**, 336 (1982).
29. Lindgård, A., Nielsen, S. E., At. Data Nucl. Data Tables **19**, 533 (1977).
30. Biémont, E., Physica **85C**, 393 (1977).
31. Flower, D. R. and Nussbaumer, H., Astron. Astroph. **42**, 265 (1975).
32. Weiss, A. W., J. Quant. Spect. Rad. Transfer **18**, 481 (1977).
33. Fawcett, B. C. (private communication).
34. Omidvar, K., Phys. Rev. **A26**, 3053 (1982).
35. Curtis, L. J., Am. J. Phys. **36**, 1123 (1968).
36. Lindgård, A. and Veje, E., Nucl. Instr. Meth. **202**, 377 (1982).
37. Nitsche, W., Heckmann, P. H., Träbert, E. and Buttlar, H. v., Z. Physik **A299**, 301 (1981).
38. Kido, Y. and Kawamoto, J., Nucl. Instr. Meth. **202**, 493 (1982).
39. Betx, H. -D., Röschenthaler, D., Rothermel, J., Phys. Rev. Lett. **50**, 34 (1983).